Available online at www.sciencedirect.com

SciVerse ScienceDirect

Ceramics International 38 (2012) 4049–4055

CERAMICS INTERNATIONAL

www.elsevier.com/locate/ceramint

Novel processing and magnetic properties of hematite/maghemite nano-particles

N.M. Deraz [a,b,*], A. Alarifi [b]

[a] Physical Chemistry Department, Laboratory of Surface Chemistry and Catalysis, National Research Center, Dokki, Cairo, Egypt
[b] Catalytic Chemistry Research Chair, Chemistry Department, College of Science, King Saud University, Riyadh, Saudi Arabia

Received 23 October 2011; accepted 11 December 2011
Available online 31 January 2012

Abstract

Hematite/maghemite nano-particles were synthesized by combustion method using different ratios of fuel. Effects of these ratios on crystalline phases, crystallite size, morphological and magnetic properties of the nano-particles have been investigated. The products were characterized by XRD, SEM and EDX techniques. Magnetic properties of the as prepared nano-particles were evaluated on a vibrating sample magnetometer. X-ray diffraction analysis indicates that low content of fuel promotes the formation of alpha ferric oxide, whereas high content of this fuel produces gamma ferric oxide with alpha ferric oxide. Varied morphology for the glycine-treated samples compared to untreated specimen was observed. The treatment with glycine brought about an increase in the concentration of ferric species at the as prepared solids as shown from EDX analysis. However, the mixture containing hematite/maghemite nano-particles led to better magnetic properties depending upon the presence of maghemite crystallites.

Keywords: α-Fe_2O_3; γ-Fe_2O_3; SEM; EDX; M_s; H_c

1. Introduction

Recently materials scientists are focusing their efforts on developing simple and effective methods for fabricating nano-materials with controlled size and morphology and hence tailoring their properties due to the strong effects of size and shape of these materials on their physical and chemical properties [1–4]. Advanced magnetic nano-particles with properties of super-para-magnetism, in addition to their low toxicity and biocompatibility, have been intensively studied because of their potential technological applications, including magnetic storage, magnetic ink printing, microwave absorption, biosensors, bio-separation, in vivo drug delivery, magnetic resonance imaging contrast agents, and hyperthermia treatment of cancer [5–10].

Iron oxide nano-particles have many advantages over different materials, e.g., better oxidative stability, compatibility in non-aqueous systems, and non-toxicity. Iron oxide has different crystalline phases, Fe_3O_4 as magnetite, γ-Fe_2O_3 as maghemite, and α-Fe_2O_3 as hematite [11]. Maghemite has gained the greatest interest in the above mentioned applications. Also, γ-Fe_2O_3 is also a technologically important compound widely used for the production of magnetic materials and catalysts [12]. Its structure is isometric, of defective spinel form, and somewhat iron-deficient. However, natural maghemite is formed by the oxidation of magnetite. In addition, gamma ferric oxide is a ferri-magnetic material that finds wide use as magnetic storage media in audio and video recording [13]. A variety of methods have been reported in the literature to synthesize iron oxide nano-particles, such as combustion, sol–gel, micro emulsion, pyrolysis and even ultrasonic-assisted methods [14].

The present work deals with the synthesis of hematite/maghemite nano-particles by using combustion method, study of the change in their structural, morphological and magnetic properties due to the treatment with different amounts of the investigated fuel.

* Corresponding author at: Catalytic Chemistry Research Chair, Chemistry Department, College of Science, King Saud University, Riyadh, Saudi Arabia. Tel.: +966 541684405.
E-mail address: nmderaz@yahoo.com (N.M. Deraz).

0272-8842/$36.00
doi:10.1016/j.ceramint.2011.12.081

2. Experimental

2.1. Preparation of nano-magnetic materials

Various iron oxide samples were prepared by mixing calculated proportions of iron nitrate with different amounts of glycine. The mixed precursors were concentrated in a porcelain crucible on a hot plate at 350 °C for 10 min. The crystal water was gradually vaporized during heating and when a crucible temperature was reached, a great deal of foams produced and spark appeared at one corner which spread through the mass, yielding a voluminous and fluffy product in the container. In addition, the as-prepared products were heat treated at 700 °C for 1 h to enhance their crystallinity and remove the residual charred organic materials. In this investigation, the ratio of the glycine: ferric nitrate were (0, 1, 2, 4 and 8): 1 for F1, F2, F3, F4 and F5 samples, respectively. The chemicals employed in the present work were of analytical grade supplied by Prolabo Company. It had been reported that the ratio of glycine to nitrate (G/N) had a strong impact on the experimental temperature and also a higher G/N ratio would lead to a higher temperature [1–4].

2.2. Characterization of the as synthesized materials

An X-ray measurement of various mixed solids was carried out using a BRUKER D8 advance diffractometer (Germany). The patterns were run with Cu K_α radiation at 40 kV and 40 mA with scanning speed in 2θ of 2° min^{-1}.

The crystallite size of Fe_2O_3 present in the investigated solids was based on X-ray diffraction line broadening and calculated by using Scherrer equation [15].

$$d = \frac{B\lambda}{\beta \cos\theta}$$

where d is the average crystallite size of the phase under investigation, B is the Scherrer constant (0.89), λ is the wave length of X-ray beam used, β is the full-width half maximum (FWHM) of diffraction and θ is the Bragg's angle.

Scanning electron micrographs (SEM) was recorded on JEOL JAX-840A electron microanalyzer. The samples were dispersed in ethanol and then treated ultrasonically in order to disperse individual particles over gold grids.

Energy dispersive X-ray analysis (EDX) was carried out on Hitachi S-800 electron microscope with an attached kevex Delta system. The parameters were as follows: accelerating voltage 15 kV, accumulation time 100 s, window width 8 μm. The surface molar composition was determined by the Asa method, Zaf-correction, Gaussian approximation.

2.3. Magnetic behavior of the investigated materials

The magnetic properties of the investigated solids were measured at room temperature using a vibrating sample magnetometer (VSM; 9600-1 LDJ, USA) in a maximum applied field of 15 kOe. From the obtained hysteresis loops, the saturation magnetization (M_s), remanence magnetization (M_r) and coercivity (H_c) were determined.

3. Results and discussion

3.1. XRD investigation

The XRD patterns of F1, F2, F3, F4 and F5 solid samples are shown in Fig. 1. Inspection of this figure revealed that: (i) the F1 specimen consisted of poorly crystalline α-Fe_2O_3 phase (rhombohedral, corundum structure). (ii) The F2 sample consisted of moderate crystalline α-Fe_2O_3 phase with subsequent increase in the height of all diffraction line related to this phase indicating the promotion effect of glycine fuel in the enhancement of the degree of crystallization of α-Fe_2O_3 crystallites. However, the F3 sample consisted of well crystalline γ-Fe_2O_3 (minor phase, cubic, and spinel structure) and α-Fe_2O_3 (major phase) solids with subsequent a progressively increase in the peak height related to all phases produced. The values of lattice constants of α-Fe_2O and γ-Fe_2O_3 were $a = b = c = 5.039$ and $a = b = c = 8.375$, respectively. (iii) Increasing the G/N ratio in the investigated solids from 1 to 2 led to an important decrease in the peak height of both α- and γ-Fe_2O_3 phases as shown in F4 sample. This finding suggests a partial conversion of α-Fe_2O_3 to γ-Fe_2O_3 phase. (iv) The augmentation in the G/N ratio up to 8 resulted in slightly increase in the peaks height of α-Fe_2O_3 as a single phase with disappearance of the diffraction line related to γ-Fe_2O_3 phase. These observations suggest the stimulation effect of glycine treatment on the phase transformation of the

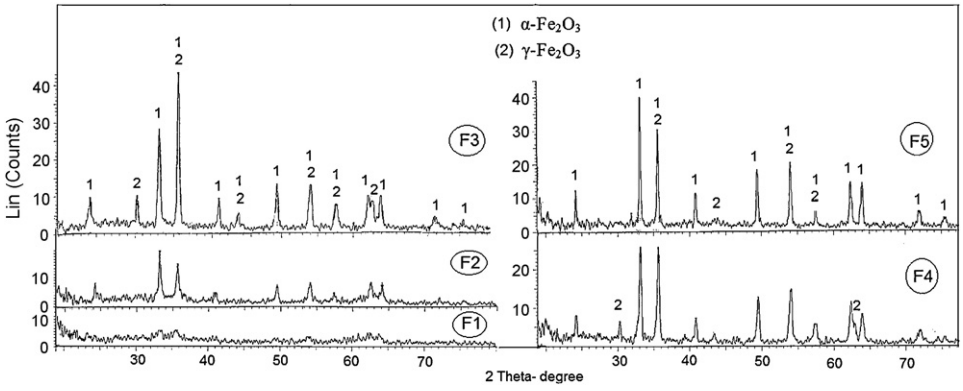

Fig. 1. X-ray diffractograms for F1, F2, F3, F4 and F5 solids.

Table 1
The effects of G/N ratio on the crystallite size of the crystalline phases involved in the as synthesized system.

Solids	G/N ratio	Crystalline phases	Crystallite size (nm)	
			α-Fe_2O_3	γ-Fe_2O_3
F1	0	α-Fe_2O_3	3	–
F2	0.5	α-Fe_2O_3	34	–
F3	1	α-Fe_2O_3 + γ-Fe_2O_3	35	32
F4	2	α-Fe_2O_3 + γ-Fe_2O_3	38	35
F5	4	α-Fe_2O_3	50	–

investigated phases. One cannot overlook the presence of Fe_3O_4 phase depending upon the similarity between the diffraction lines of both γ-Fe_2O_3 and Fe_3O_4 phases. From X-ray analysis, the lattice parameter calculated for the peak at 0.295 nm is 0.8348 nm, which is very close to the lattice parameter (0.8350 nm) reported for maghemite (γ-Fe_2O_3), and different to magnetite (Fe_3O_4), with a reported lattice parameter of 0.8396 nm. Thus we can conclude that the F1, F2 and F5 samples consisted of crystalline α-Fe_2O_3 phase only whereas the F3 and F4 samples contain a mixture of α-Fe_2O_3 and γ-Fe_2O_3 phases as shown in Table 1. (v) The crystallite size of various phases increases by increasing of the G/N ratio as listed in Table 1. In fact, the γ-crystallites obtained showed sizes similar to that of α-crystallite. With continuous heating, the α-Fe_2O_3 coarsened to a size of 50 nm. However, the peak height of the diffraction lines at d-spacing 0.295 and 0.270 nm were considered as a measure of the degree of crystallinity of γ-Fe_2O_3 and α-Fe_2O_3 phases, respectively. The values of height of the lines at 0.295 and 0.270 nm are listed in Table 2. It is clear from this table that the increase in the G/N ratio brought about an increase in the degree of crystallinity of different phases. (vi) With increasing the content of glycine added, a progressive shift of all diffraction peaks to higher Bragg angle was observed. This shift displays presence of changes in both the crystallinity and crystallite size of the investigated solids. The observed increase in the crystallite size of the resulting oxides could be attributed to an increase in the flame temperature which assists crystal growth and/or the redistribution of cations in crystal structure of these oxides.

The enhancement effects of the G/N ratio on the phase transformation process are better investigated by measuring the height of certain diffraction lines characteristic for α-Fe_2O_3 (0.270 nm, 100%) and relative to one the common lines of both α-Fe_2O_3 (0.251, 75%) and γ-Fe_2O_3 (0.251, 100%). This was done and the results obtained are given in Table 2. Inspection of this table revealed that: (i) The ratio, *R*, between the peak height of the lines at "d" spacing of 0.251 and 0.270 nm for the F1 sample was 0.750 which is the same of pure α-Fe_2O_3 (0.75). This indicates absence of γ-Fe_2O_3 phase. (ii) The addition of small amount of glycine led to a smallest increase (2.66%) in the value of R indicating to the formation of γ-Fe_2O_3 phase due to a partial conversion of some α-Fe_2O_3 to γ-Fe_2O_3 phase. (iii) Increasing the G/N ratio in the investigated solids from 0.5 to 2 led to an important increase in the *R* value which decreases above this limit but it is still greater than that of pure α-Fe_2O_3 phase. Higher value of *R* was obtained when G/N = 2 indicating to the enhancement of γ-Fe_2O_3 formation due to glycine treatment. These observations indicate that the F2 and F5 samples maybe contain amorphous γ-Fe_2O_3 phase and nano-crystalline α-Fe_2O_3 phase.

Table 2
The effects of G/N ratio on the height of some lines at 'd' spacing of 0.270 nm (100% α-Fe_2O_3) and 0.251 nm (75% α-Fe_2O_3 + 100% γ-Fe_2O_3) involved in XRD pattern of the investigated system.

Solids	G/N ratio	Peak height (au)		Ratio between b/a (*R*)
		0.270 nm (a)	0.251 nm (b)	
F1	0	6.4	4.8	0.750
F2	0.5	18.3	14.1	0.770
F3	1	27.9	42.8	1.534
F4	2	26.6	25.9	0.974
F5	4	40	32	0.800

3.2. Morphology study

The crystallite size and morphology of the prepared powder were checked by SEM analysis with different magnifications as shown in Figs. 2–5. The measured crystal size was in a good

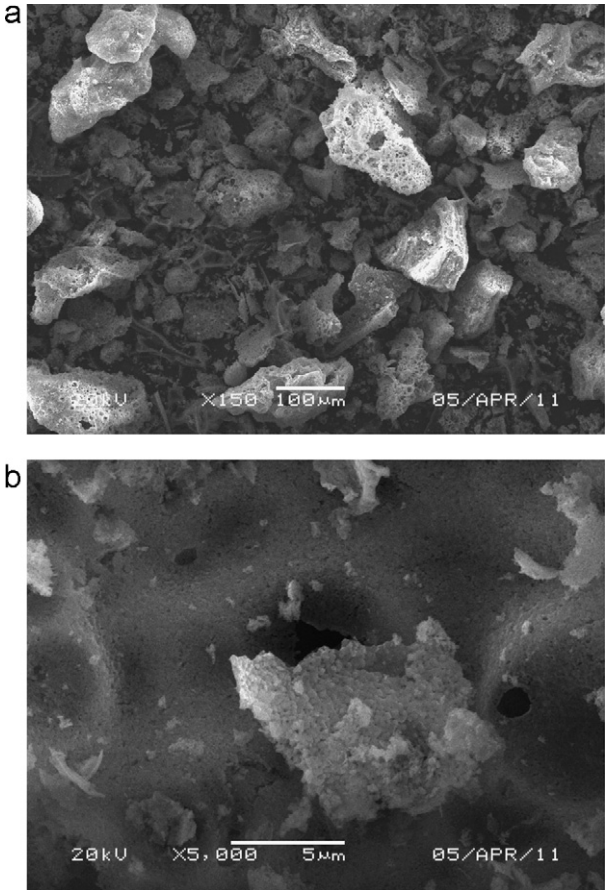

Fig. 2. SEM images for the F1 sample with different magnifications: (a) 150; (b) 5000.

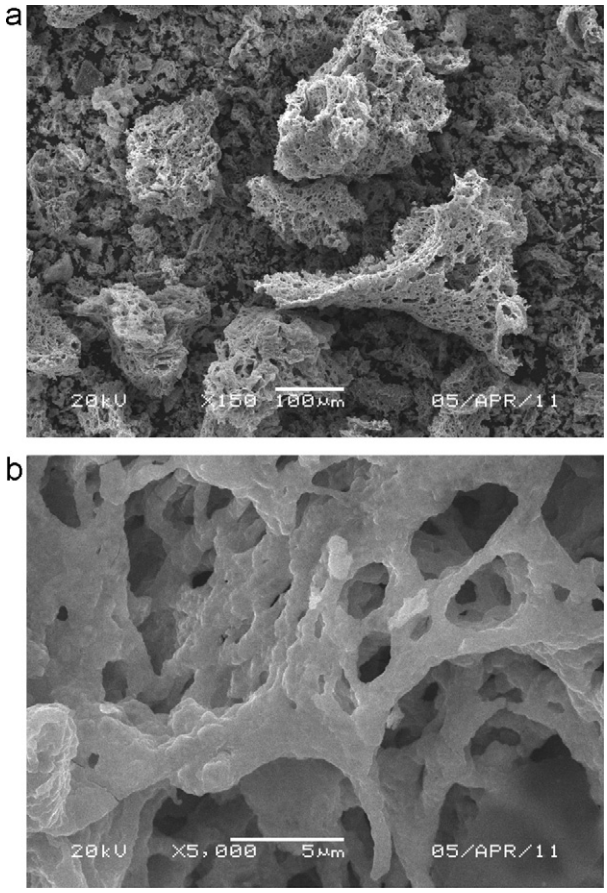

Fig. 3. SEM images for the F3 sample with different magnifications: (a) 150; (b) 5000.

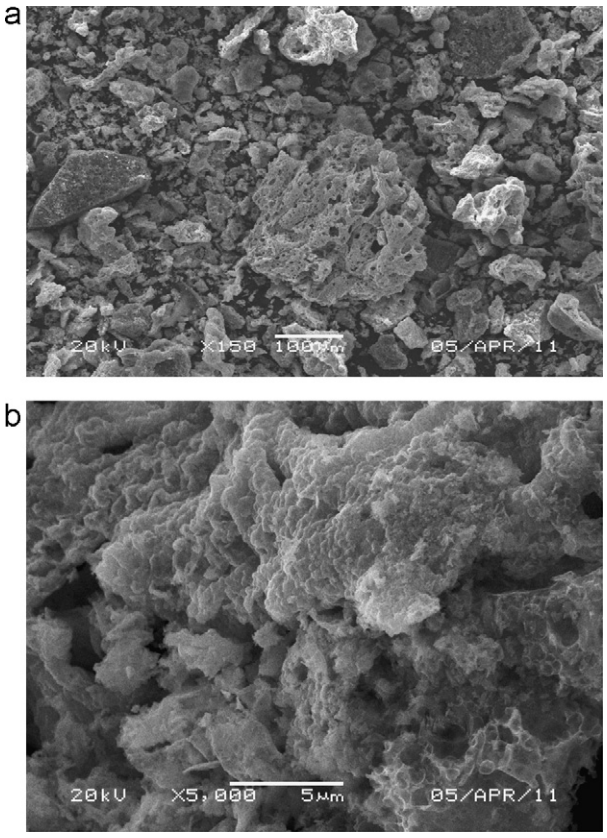

Fig. 4. SEM images for the F4 sample with different magnifications: (a) 150; (b) 5000.

agreement with XRD data. Fig. 2a and b shows Fe_2O_3 particles of pseudo-spherical shape obtained in the absence of the fuel. I can see from this figure that the powder was formed in irregular and agglomerated nano-sized Fe_2O_3 particles which seem to be developed in a dense structure with macro and microspores. The size and morphology of Fe_2O_3 particles were strongly influenced by adding glycine to the as prepared system. Figs. 3–5 reveal remarkable changes in the microstructure, regarding grain size, porosity and the particle distribution of the as-prepared solids by changing the heat treatment conditions depending on the ratio between glycine and nitrates. However, the presence of voids and pores in the samples are attributed to the release of large amount gases during combustion process. In the F3, F4 and F5 samples one can see the formation of multigrain agglomerations consisted of spongy structure crystallites. The microstructure of the prepared powder shows two types of aggregates with different grain sizes depending upon the increase in the glycine content. One type consists of dense matrix constituting the majority of the sample, while the second type consists of smaller grains which is more likely to agglomerated maghemite. The compact are characterized by both open macro and micropores at the surface and also by a dense matrix of Fe_2O_3 in the bulk. The increase in the crystal size brought about an increase in the number of macropores. Opposite behavior was observed in the case of micropores.

3.3. EDX investigation

Energy dispersive X-ray (EDX) analysis of various ferric oxide specimens was carried out. The relative atomic abundance of Fe and oxygen species present in the uppermost surface layers of various solids is given in Table 3. It is well known that EDX technique supplies the effective atomic concentration of different constituents of the solids investigated present on their top surface layers.

Inspection of Table 3 reveled that: (i) The surface O/Fe ratio in the solids prepared by combustion route was strongly dependent on the amount of glycine added. (ii) The surface concentrations of Fe in all solids investigated are bigger than that in the bulk of these solids. (iii) Increasing amounts of glycine gave lower surface O/Fe ratio. These findings suggest a possible migration of some of Fe species from the bulk towards the surface of the solids. However, the decrease in the concentration of oxygen species maybe indicates the formation of maghemite species at solid surface depending on the crystal structure of maghemite. In magnetite and maghemite, the oxygen ions are in a cubic close-packed arrangement. Magnetite has an inverse spinel structure with Fe(III) ions distributed randomly between octahedral and tetrahedral sites, and Fe(II) ions in octahedral sites [16]. Maghemite has a spinel structure that is similar to that of magnetite but with vacancies in the cation sublattice. Haneda and Morrish [17] found that the

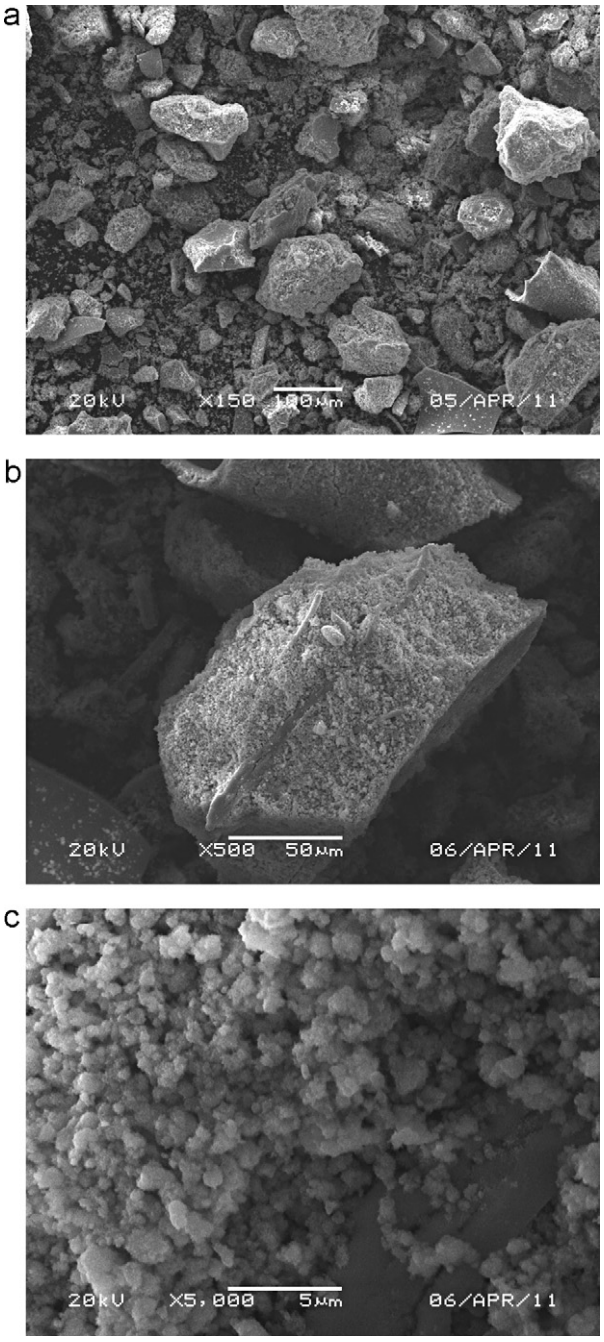

Fig. 5. SEM images for the F5 sample with different magnifications: (a) 150; (b) 500; (c) 5000.

degree of vacancy ordering decreases with decreasing particle size, with no vacancy ordering in maghemite smaller than about 20 nm.

3.4. Magnetic properties

Magnetic measurements were done at room temperature on a VSM with a peak field of 15 kOe. The hysteresis loops for different samples prepared by combustion method are shown in Fig. 6. The magnetic parameters were summarized in Table 4. Examination Table 3 revealed that: (i) The F1 sample exhibit a saturation magnetization (M_s) of 1.54 emu/g, this is much smaller compared with that of the F2, F3, F4 and F5 samples. It is found that the increase tendency of M_s is consistent with the improvement of crystallinity and phase transformation of the investigated oxides. (ii) The addition of small amount of glycine during the preparation of solids led to slightly increase in M_s, M_r and H_c of the as prepared oxides. (iii) Increasing the G/N ratio in the investigated solids from 1 to 2 led to an important increase in the values of M_s, M_r, H_c and squareness ratio (M_r/M_s) for the as synthesized solids. The maximum increase was observed in case of the F3 sample. Increasing the G/N ratio above 2 led to a decrease in the values of M_s, M_r, H_c and M_r/M_s ratio. It is found that the increase tendency of M_s, M_r, H_c and M_r/M_s ratio are consistent with the improvement of crystallinity and/or phase transformation of the investigated oxides. However, the formation of γ-Fe_2O_3 (maghemite) phase endowed with a high saturation magnetization [16]. But the saturation magnetization of γ-Fe_2O_3 nano-crystallites is significantly lower than that of bulk γ-Fe_2O_3 (76 emu/g) [18], which can probably be attributed to the nanoscale dimension and the surface defects [18–21].

The particle size and crystallinity have been reported to influence the magnetic properties of materials [1–4]. It was found that M_s decreases with decreasing crystallite size for mono-domain particles due to the surface spin canting and thermal fluctuation. In our experiments, it should not be responsible for the saturation magnetization difference observed in the investigated samples. Because the F3 sample derived from combustion process with G/N = 2, consisting of α-Fe_2O_3 and γ-Fe_2O_3 nano-particles, possesses a saturation magnetization value of 18.58 emu/g. So, we can seen that the improved crystallinity of

Table 3
EDX determination of the Surface and bulk molar concentration of ferric oxide prepared by combustion method.

Solids	G/N ratio	Elements	Atomic abundance (%)		Surface O/Fe ratio
			Calculated (bulk)	Found (surface)	
F1	0	Fe	69.94	69.73	0.431
		O	30.06	30.05	
F2	0.5	Fe	69.94	71.84	0.392
		O	30.06	28.16	
F3	1	Fe	69.94	73.74	0.356
		O	30.06	26.26	
F4	2	Fe	69.94	75.53	0.324
		O	30.06	24.47	
F5	4	Fe	69.94	77.73	0.287
		O	30.06	22.27	

Table 4
The effects of G/N ratio on the magnetic properties (M_s, M_r and H_c) of the as-prepared solids.

H_c (Oe)	M_r/M_s (emu/g)	M_r (emu/g)	M_s (emu/g)	G/N ratio	Solids
F1	0	1.536	0.009	0.006	25
F2	0.5	2.895	0.235	0.081	87
F3	1	18.580	5.480	0.295	196
F4	2	14.890	3.850	0.259	131
F5	4	4.538	0.973	0.214	174

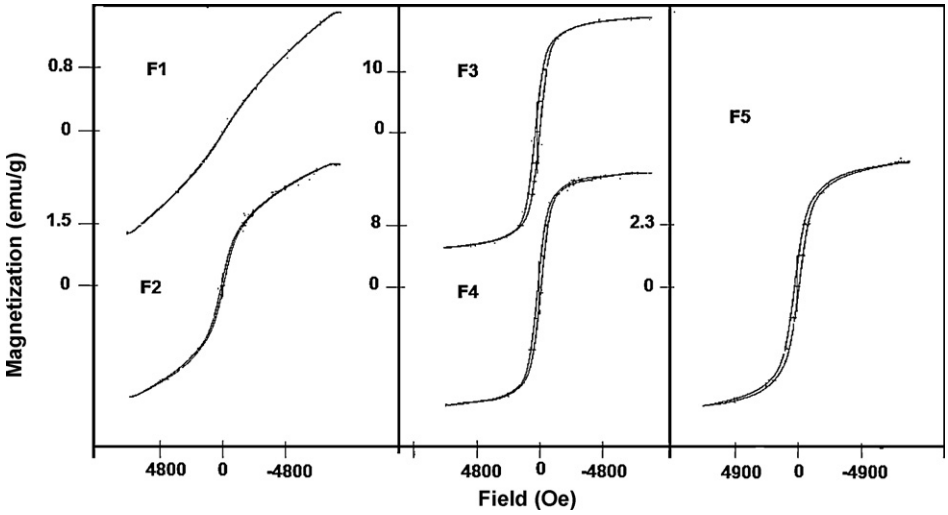

Fig. 6. Magnetic hysteresis curves measured at a room temperature for F1, F2, F3, F4 and F5 solids.

the magnetic materials, not the particle size increasing, is the main contributing factor to the observed increase of M_s and H_c in Fe_2O_3 nano-particles. Similar result of strong correlation between the crystallinity and the magnetic properties has been reported in barium ferrite powder [22,23]. One cannot overlook the effect of the formation of γ-Fe_2O_3 crystallites in an increase of the saturation magnetization.

4. Conclusions

The method of synthesis of Fe_2O_3 nano-particles by combustion process was investigated with a focus on the control of the size and the nature of Fe_2O_3 nano-crystallites. It was clarified that the amount of fuel used in the synthesis process played an important role in determining the particle size and phase transformation of the iron oxides. Formation/transformation of phases at different concentration of glycine was confirmed by XRD anlysis. Investigations, obtained by SEM and EDX showed the morphology and nano-crystal formation of hematite and maghemite. In particular, α-Fe_2O_3 nano-particles approximately 3–50 nm in diameter were synthesized via thermal decomposing of ferric nitrate or/and by its treatment with glycine, while γ-Fe_2O_3 solid measuring 32–35 nm in diameter was synthesized by combustion method. Furthermore, it was demonstrated that magnetic properties of the Fe_2O_3 nano-particles can be controlled by the ratio between the amounts of both fuel and metal nitrate.

Acknowledgement

This work was supported by NPST program by King Saud University Project: Number 09-ADV651-02.

References

[1] N.M. Deraz, Glycine-assisted fabrication of nanocrystalline cobalt ferrite system, J. Anal. Appl. Pyrol. 88 (2010) 103.
[2] N.M. Deraz, Size and crystallinity-dependent magnetic properties of copper ferrite nano-particles, J. Alloys Compd. 501 (2010) 317.
[3] N.M. Deraz, S. Shaban, Optimization of catalytic, surface and magnetic properties of nanocrystalline manganese ferrite, J. Anal. Appl. Pyrol. 86 (2009) 173.
[4] N.M. Deraz, S.A. Shaban, A. Alarifi, Removal of sulfur from commercial kerosene using nanocrystalline $NiFe_2O_4$ based sorbents, J. Saudi Chem. Soc. 14 (2010) 357.
[5] S. Laurent, D. Forge, M. Port, A. Roch, C. Robic, L. Vander Elst, R.N. Muller, Magnetic iron oxide nanoparticles: synthesis, stabilization, vectorization, physicochemical characterizations, and biological applications, Chem. Rev. 108 (2008) 2064.
[6] J.-M. Tulliani, C. Baroni, C. Lopez, L. Dessemond, New NO_x sensors based on hematite doped with alkaline and alkaline-earth elements, J. Eur. Ceram. Soc. 13 (2011) 2357.
[7] A. Ito, M. Shinkai, H. Honda, T. Kobayashi, Medical application of functionalized magnetic nanoparticles, J. Biosci. Bioeng. 100 (2005) 1.
[8] H. Choi, S.R. Choi, R. Zhou, H.F. Kung, I.W. Chen, Iron oxide nanoparticles as magnetic resonance contrast agent for tumor imaging via folate receptor-targeted delivery, Acad. Radiol. 11 (2004) 996.
[9] S.-P. Lin, J.J. Brown, MR contrast agents: physical and pharmacologic basics, J. Magn. Reson. Imaging 25 (2007) 884.
[10] M. Brahler, R. Georgieva, N. Buske, A. Muller, S. Muller, J. Pinkernelle, U. Teichgraber, A. Voigt, H. Baumler, Magnetite-loaded carrier erythrocytes as contrast agents for magnetic resonance imaging, Nano. Lett. 6 (2006) 2505.
[11] R.M. Cornell, U. Schwertmann, The Iron Oxides: Structure, Properties, Reactions, Occurrences and Uses, second ed., Wiley-VCH, Weinheim, 2003.
[12] J. Tucek, R. Zboril, D. Petridis, Maghemite nanoparticles by view of Mössbauer spectroscopy, J. Nanosci. Nanotechnol. 6 (2006) 926.
[13] D. Predoi, V. Kuncser, G. Filoti, Magnetic behaviour of maghemite study by Mössbauer spectroscopy, Rom. Rep. Phys. 56 (2004) 373.
[14] M.H. Khedr, M. Bahgat, M.I. Nasr, E.K. Sedeek, CO_2 decomposition over freshly reduced nanocrystalline Fe_2O_3, Colloid Surf. A 302 (2007) 517.
[15] B.D. Cullity, Elements of X-ray Diffraction, Addison-Wesly Publishing Co. Inc., 1976 (Chapter 14).
[16] S. Klotz, G. Steinle-Neumann, T. Strassle, J. Philippe, T. Hansen, M.J. Wenzel, Magnetism and the Verwey transition in Fe_3O_4 under pressure, Phys. Rev. B 77 (2008) 012411.
[17] K. Haneda, A.H. Morrish, vacancy ordering in γ-Fe_2O_3 small particles, Solid State Commun. 22 (12) (1977) 779.

[18] Z.-H. Jing, S.-H. Wu, Synthesis, characterization and magnetic properties of γ-Fe_2O_3 nanoparticles via a non-aqueous medium, J. Solid State Chem. 177 (2004) 1213.

[19] B. Hong, C. Qianwang, S. Tao, Preparation of ferromagnetic γ-Fe_2O_3 nanocrystallites by oxidative co-decomposition of PEG 6000 and ferrocene, Solid State Commun. 141 (2007) 573.

[20] R. Zboril, L. Machala, M. Mashlan, V. Sharma, Iron(III) oxide nanoparticles in the thermally induced oxidative decomposition of Prussian blue, $Fe_4[Fe(CN)_6]_3$, Cryst. Growth Des. 4 (2004) 1317.

[21] C.J. Serna, F. Bődker, S. Mőrup, M.P. Morales, F. Sandiumenge, S. Veintemillas-Verdaguer, Spin frustration in maghemite nanoparticles, Solid State Commun. 118 (2001) 437.

[22] M.S. Chen, Z.X. Shen, X.Y. Liu, J. Wang, Raman and magnetization studies of barium ferrite powder prepared by water-in-oil microemulsion, J. Mater. Res. 15 (2000) 483.

[23] C.A. Barrero, R.E. Vandenberghe, E. De Grave, The effect of Al-content and crystallinity on the magnetic properties of goethites, Hyperfine Interact. 122 (1999) 39.